ACS OMEGA

Open Access

http://pubs.acs.org/journal/acsodf

Article

Statistically Analyzed Heavy Metal Removal Efficiency of Silica-Coated $Cu_{0.50}Mg_{0.50}Fe_2O_4$ Magnetic Adsorbent for Wastewater Treatment

Published as part of ACS Omega virtual special issue "Magnetic Nanohybrids for Environmental Applications".

Muhammad Irfan, Anam Arif, Muhammad Adnan Munir, Muhammad Yasin Naz,* Shazia Shukrullah, Saifur Rahman, Mohammed Jalalah, and Abdulkarem H. M. Almawgani

Cite This: *ACS Omega* 2023, 8, 47623−47634

Read Online

ACCESS | Metrics & More | Article Recommendations

ABSTRACT: Even low concentrations of pollutants in water, particularly heavy metals, can significantly affect the ecosystem and human health. Adsorption has been determined to be one of the most effective techniques of removing pollution from wastewater among the various strategies. To remove heavy metals such as Zn^{2+} and Pb^{2+}, we prepared a silica-coated $CuMgFe_2O_4$ magnetic adsorbent using sol−gel method and tested it for wastewater treatment. X-ray diffraction investigation validated the creation of cubic spinel structure, while morphological analysis showed that silica coating reduces the particle size but boosts the surface roughness of the nanoparticles and also reduces the agglomeration between particles. UV−visible spectroscopy indicates a rise in bandgap and magnetic characteristics analysis indicates low values of magnetization due to silica coating. The kinetic and isotherm parameters for heavy metal ions adsorption onto silica-coated $Cu_{0.50}Mg_{0.50}Fe_2O_4$ nanoparticles are calculated by applying pseudo-first-order, pseudo-second-order, Langmuir and Freundlich models. Adsorption kinetics revealed that the pseudo-second-order and Langmuir models are the best fit to explain adsorption kinetics. Synthesized adsorbent revealed 92% and 97% removal efficiencies for Zn^{2+} and Pb^{2+} ions, respectively.

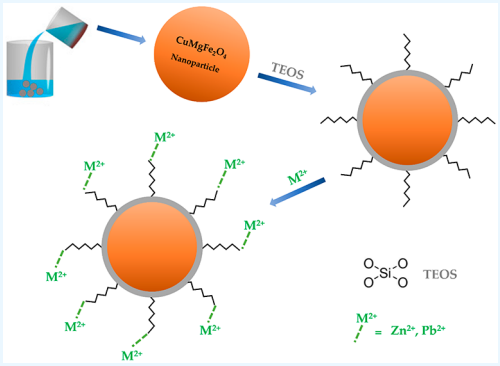

1. INTRODUCTION

The uncontrolled discharge of polluted water from the chemical and metal processing industries causes the accumulation of toxic elements in freshwater reserves. The existence of synthetic dyes, drugs, pesticides, petroleum hydrocarbons, and heavy metals contaminants adversely affects water's purity, which is a major threat to aquatic life and humans.[1] Even low concentrations of heavy metals can cause adverse effects on human and aquatic species.[2] Thallium is the main cause of alopecia in humans; Minamata disease is caused by mercury. Cadmium is the source of itai-itai disease, and lead poisoning causes intellectual abnormality in children.[3] Pollutants in water are classified as either point or nonpoint sources. Pollution in the former case comes from a single identifiable source, whereas pollution in the latter case comes from various sources.[4] Pollutants are generally classified into suspended solids and sediment, radioactive, microorganism, nutrients, inorganic, and organic, depending on their key physicochemical characteristics. Heavy metals, ammonia, fertilizers, sulfides, acids, bases, and nitrogen oxides are typical examples of inorganic pollutants.[5] Heavy metals have densities larger than 5 g/cm^3.[3,6] These metals, unlike organic pollutants, are highly toxic and carcinogenic. Heavy metals do not degrade and tend to build up in organisms.[7] As a result, heavy metals' exposure via potable water has remained a major concern of public health worldwide.[8] Zinc, nickel, copper, chromium, arsenic, cadmium, lead, and mercury are some well-known heavy metals.

Heavy metals from industrial influents have been eliminated from wastewater for decades by using common treatment technologies, including electrochemical removal,[9] ion flotation,[10] coagulation,[11] solvent extraction,[12] and adsorption methods.[13] Various substances, including chitosan, zeolite, ferrites, resins, and activated carbon, have been used for wastewater treatment.[14] In the current scenario, magnetic materials have drawn much attention, because of their exceptional characteristics and possible use in wastewater

Received: August 6, 2023
Revised: November 7, 2023
Accepted: November 10, 2023
Published: December 8, 2023

Figure 1. Illustration of synthesis and silica coating of $Cu_{0.50}Mg_{0.50}Fe_2O_4$ adsorbent.

treatment. The magnetic separation method is extensively utilized for wastewater treatment due to its reusability for many cycles. Nonmagnetic nanoparticles are less effective in treating industrial effluents because of difficulty of separating from the aqueous phase and small reactive surface area.[15] Ferrite nanomaterials have several advantages over conventional adsorbents as they exhibit tremendous adsorption capacity and chemical stability, even at high temperatures. Moreover, ferrites can be designed with specific characteristics, allowing the adoption of selective species from aqueous media.[16] However, ferrite nanoparticles can oxidize under acidic conditions and aggregate due to the magnetic effect. Coating ferrite nanoparticles, in many cases, is done to avoid the oxidation problem. Magnetic nanoparticles are frequently coated with substances, such as inorganic compounds, polymeric materials, or hybrid materials, to increase their effectiveness and stability. Consequently, encapsulating magnetic nanoparticles is a crucial tactic for inhibiting the direct interactions of the magnetic nanoparticles.[17] In silica-coated magnetic adsorbents, silanol (−SiOH) and other hydroxyl groups on the absorbent form complexes with heavy metal ions to immobilize these metal ions on the adsorbent nanoparticles. The Langmuir and Freundlich isotherms are also used to get insights into the affinity and adsorption capacity of adsorbents for selected heavy metal ions. Therefore, both adsorption isotherms were studied to deduce an effective adsorption mechanism of the tested silica-coated $CuMgFe_2O_4$ adsorbent. This study focuses on the removal of lead and zinc metals from wastewater. Lead is a toxic metal with severe environmental and health related issues. It is imperative to reduce exposure to lead ions to protect human health and the environment. Zinc, when properly managed, can be beneficial for various biological processes. It is an essential human nutrient with limited environmental impact when available within acceptable levels. Excessive zinc intake through contaminated water and food can lead to gastrointestinal disturbances and impair the absorption of other minerals like copper and iron. The zinc in water bodies can also be toxic to aquatic life, particularly sensitive species such as fish and aquatic invertebrates. Zinc in the soil affects plant growth and enters the food chain.

In the published literature, Liu et al.[18] reported that $MgFe_2O_4$ nanoparticles perform well in removing basic fuchsin dye and methyl green from wastewater. Naz et al.[19] investigated the optical properties, structure and magnetic response of $MgFe_2O_4$ nanoparticles for dye removal from the wastewater. The ferrite nanoparticles were given nonthermal plasma treatment to make the surface more porous and reactive. The plasma-treated nanoparticles revealed 97% dye removal from the solution compared to 93% removal by the pristine nanoparticles. Tang et al.[20] reported that $Mg_{0.27}Fe_{2.50}O_4$ nanoadsorbents exhibit a higher surface area than ultrafine α-Fe_2O_3 nanoadsorbents produced using the same solvent thermal processing method. The magnesium doping improved the adsorption of the sample for both As(V) and As(III) pollutants. The use of suitably surface-functionalized ferrite nanoparticles as nanoadsorbents seems attractive due to their vast surface area, strong magnetization, and good selectivity. Shukrullah et al.[21] revealed that the chemisorption property of the nanomaterials could be improved by attaching the amine groups to the surface of the nanostructures. In this work, we have chosen Cu^{2+} and Mg^{2+} as dopants to construct the $CuMgFe_2O_4$ adsorbent. The Cu^{2+} and Mg^{2+} ions with larger ionic radii are substituted between the Fe and the O sites. Cu and Mg are occasionally favored over other metals in preparing composite ferrite adsorbents for treating heavy metal ions from wastewater due to their particular features and potential to improve adsorbent performance. Cu and Mg are relatively cost-effective metals, making them attractive for adsorbent materials. These metals can provide good magnetic characteristics to the ferrite adsorbent, allowing it to be easily separated from the treated water by using some external field. It streamlines the recovery process and makes wastewater treatment more efficient. Cu^{2+} and Mg^{2+} ions have large ionic radii that are replaced between the Fe and the O sites. This substitution enhances the active surface area for heavy metal ion adsorption from wastewater. The large surface area of silica-coated $CuMgFe_2O_4$ provides plenty of active sites for heavy metal ions to adsorb onto the material. Combining metal oxides (Cu, Mg, Fe) and silica increases its adsorption capacity, allowing it to remove heavy metals.[22] Under diverse environmental conditions, silica-coated $CuMgFe_2O_4$ demonstrates good stability. It is cost-effective for long-term heavy metal remediation activities, because it may be regenerated and reused several times.

https://doi.org/10.1021/acsomega.3c05764
ACS Omega 2023, 8, 47623−47634

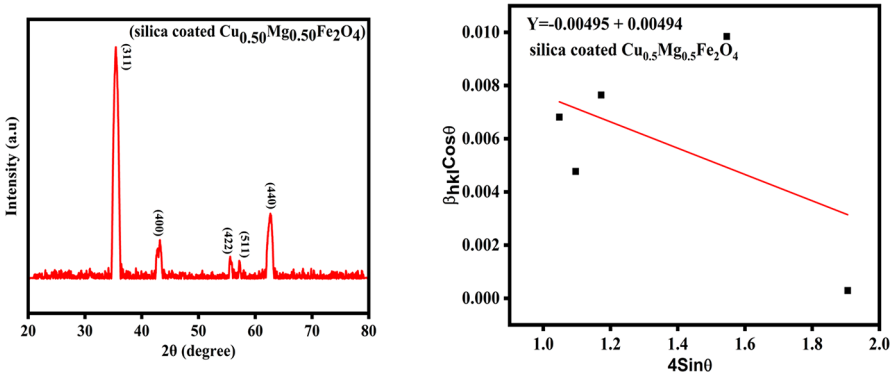

Figure 2. XRD spectrum and Williamson Hall plot for microstrain of the silica-coated $Cu_{0.50}Mg_{0.50}Fe_2O_4$ adsorbent.

2. MATERIALS AND METHODS

2.1. Synthesis of Ferrite Adsorbent. A facile sol−gel method was adopted to synthesize $Cu_{0.50}Mg_{0.50}Fe_2O_4$, as illustrated in Figure 1. In the first step, Fe, Cu, and Mg metal chlorides were dissolved in deionized water in the required stoichiometric ratios. After that, the citric acid solution was prepared separately by utilizing 2.22 mol of citric acid ($C_6H_8O_7$) and 60 mL of deionized water. Afterward, the citric acid solution was introduced to the metal chloride solution under vigorous stirring. The acquired solution was then continuously stirred for 2 h at 60 °C. After mixing metal chlorides and citrate solution, ammonium hydroxide was added to adjust the pH of the solution at 7. Continuous stirring and heating of the acquired solution resulted in the formation of sol, which was further converted into gel after heating for 8 h. The produced gel was then dried at 100 °C for 6 h and subsequently calcined at 600 °C for 6 h. After calcination, the obtained matrix was finely ground into powder. The prepared ferrite specimen was then coated with silica using tetraethyl silicate. A powdered ferrite sample was introduced in distilled water and then tetraethyl orthosilicate silane was added dropwise for direct silanization of ferrite adsorbent. The sample was then treated ultrasonically for 10 min and then stirred for 2 h. Silica-coated $Cu_{0.50}Mg_{0.50}Fe_2O_4$ was obtained after heating the obtained slurry for 3 h at 300 °C.

2.2. Characterization Techniques. The structure and crystallite size of the synthesized samples, along with the lattice parameters, were investigated through XRD analysis. Bruker D8 equipment with Cu Kα radiation, having wavelengths of 1.54 Å, was operated at 40 kV to produce XRD spectra. SEM Nova-Nano 450 SEM instrument was used to study the morphology of pristine and silica-coated ferrites. TEM images were produced to check the internal structure and interlayer spacing of the nanostructures. FTIR spectra of ferrite samples were generated by using an Agilent Cary-630 spectrometer. Optical absorption spectra were obtained with a UV/vis spectrometer (Perkin Lambda 25). Lakeshore-7410 (VSM) was utilized to examine the magnetic attributes of the uncoated and silica-coated ferrites.

2.3. Adsorption Process. To simulate the wastewater, 0.02 g of zinc acetate and lead nitrate were added to 100 mL of deionized water. Then, 0.25 g of silica-coated $Cu_{0.50}Mg_{0.50}Fe_2O_4$ adsorbent was dissolved in the simulated wastewater to conduct the adsorption experiments. The prepared solution was continuously stirred for 1 h after maintaining pH at 7 and supernatants were filtered using filter paper. AAS (atomic adsorption spectroscopy) was used to analyze the residual heavy metal concentrations in supernatants. The kinetic parameters for heavy metal ions adsorption onto silica-coated $Cu_{0.50}Mg_{0.50}Fe_2O_4$ nanoparticles were calculated by applying pseudo-first-order and pseudo-second-order kinetics. The Langmuir and Freundlich isotherms were also used to gain insights into the affinity and adsorption capacity of adsorbents for selected heavy metal ions.

3. RESULTS AND DISCUSSION

3.1. XRD Analysis of Adsorbent. The XRD spectrum of silica-coated $Cu_{0.50}Mg_{0.50}Fe_2O_4$ is presented in Figure 2. The formation of (311), (400), (422), (511), and (440) planes at 2θ values of 35.4°, 43.2°, 55.5°, 57.8°, and 62.7° confirm the production of cubic spinel structure of $Cu_{0.50}Mg_{0.50}Fe_2O_4$.[23] Equation 1 was used to calculate the lattice constant.

$$a = d(h^2 + k^2 + l^2)^{1/2} \quad (1)$$

The lattice constant was estimated as 8.36 Å, which is slightly lower than the reported value in the literature.[24] The small value of the lattice parameter can be due to a difference in crystal structure and thermal expansion coefficient of silica and ferrite that resulted in defects and dislocations at the interface.[25] The size of the crystallite was estimated by using the Scherrer equation:

$$D = (k\lambda/\beta \cos\theta) \quad (2)$$

The crystallite size of silica-coated $CuMgFe_2O_4$ was measured to be 23 nm, slightly lower than the crystallite size of pristine ferrite. Silica coating generates a barrier to crystal growth and prevents aggregation by reducing surface energy, consequently reducing crystallite size.[26,27] Such reduction in crystallite size results in an increased surface area to volume ratio of ferrites, which consequently offers excessive active sites and upsurges the absorption capacity of composite ferrite adsorbents for heavy metals.[28] Leal et al.[26] performed surface treatment MFe_2O_4 (M = Cu, Ni, Co, Mn, and Fe) spinal ferrites through silanization and chitosan functionalization. The surface modification significantly influenced the crystallite size. The size decreased after silanization of the spinal ferrites for all substituted metals. The chitosan functionalization further reduced the crystallite size. Zeb et al.[29] revealed that a decrease in crystallite size of the surface-treated ferrite nanoparticles might be due to the high nucleation rate of nanocrystals in the silane matrix. Fast nucleation suppresses the growth of crystallites. Saturation magnetization was also reported to be lower in pristine ferrite nanoparticles than SiO_2

https://doi.org/10.1021/acsomega.3c05764
ACS Omega 2023, 8, 47623−47634

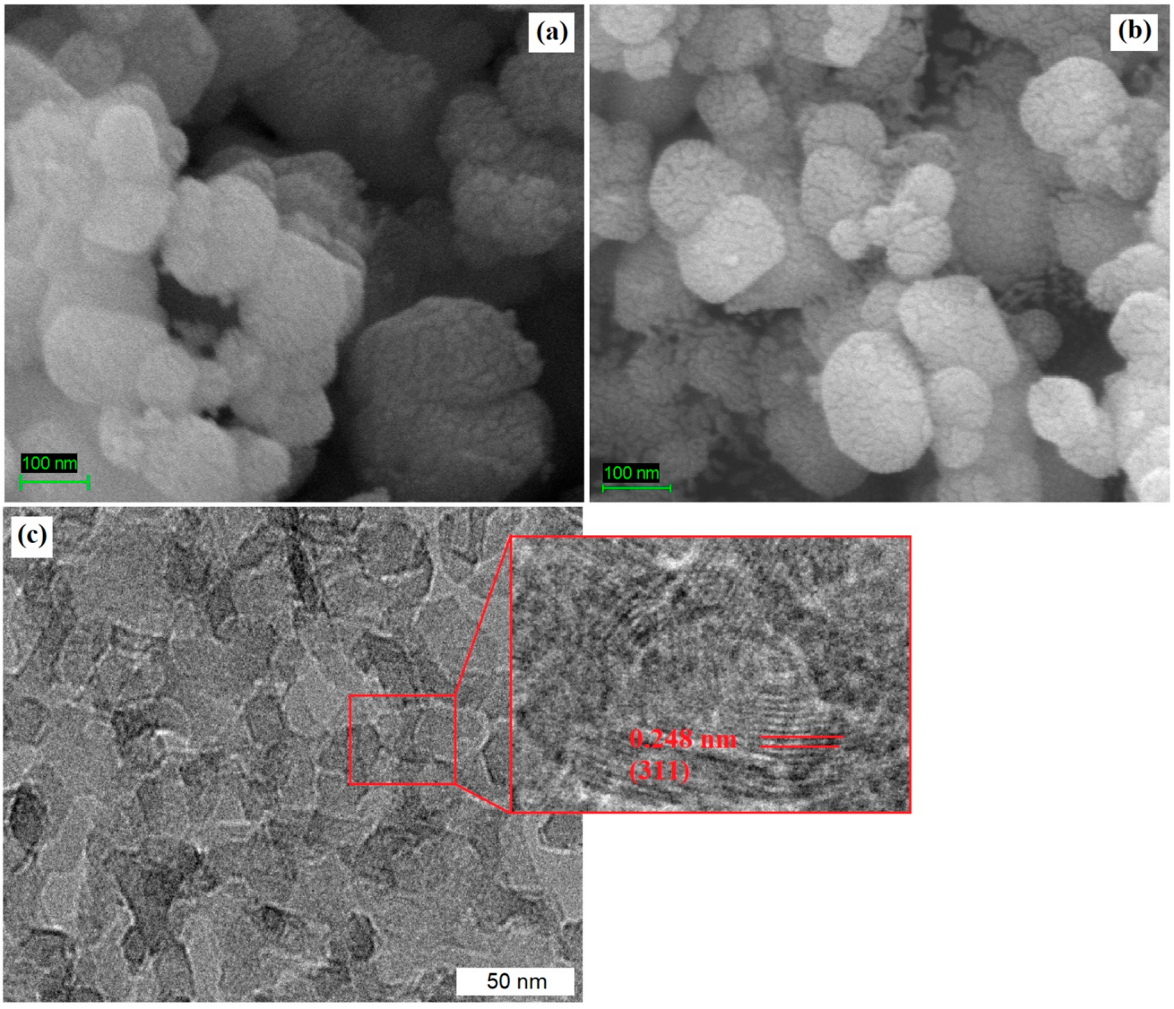

Figure 3. (a) SEM micrographs of the pristine adsorbent and (b) silica-coated adsorbent and (c) TEM image of the silica-coated adsorbent.

modified nanoparticles due to magnetically nonresponsive surface covering of pristine adsorbent nanoparticles. The modified nanoparticles showed high surface anisotropy compared to pristine nanoparticles due to weak dipolar interactions among the modified nanoparticles. Ferrer et al.[27] modified the structural and surface properties of $NiFe_2O_4$ with SiO_2−silane coating for adsorption of Cu^{2+} ions from wastewater. It was revealed that the crystallite size growth shows a linear relation with the temperature. The crystallite size followed the Ostwald ripening process. The growth in particle size is due to agglomeration of smaller particles, which are energetically less stable. The agglomerated particles reduce the limits of the interface and surface energy. It is worth mentioning that the redistribution of cations at octahedral and tetrahedral sites of a spinal structure and the formation of a hematite phase impurity may also affect the crystallite size.

Dislocations are the asymmetry in a crystal, which occurs due to mismatch of lattice from one part to another part with in a crystal.[30] The dislocation density (δ) and strain (ε) of synthesized samples were calculated by eqs 3 and 4, while eq 5 is Williamson−Hall's term that is used to plot the microstrain graph.

$$\delta = 1/D^2 \tag{3}$$

$$\varepsilon = \frac{\beta}{4 \tan \theta} \tag{4}$$

$$\beta_{hkl} \cos \theta = \frac{K\lambda}{D} + 4\varepsilon \sin \theta \tag{5}$$

Figure 2 exhibits a Williamson−Hall plot for the prepared sample. The microstrain is obtained from the slope of the linearly fitted data and the crystallite size is obtained from the root of the y-intercept. The dislocation density and microstrain were calculated as 0.03905 and -4.35×10^3, respectively. The total strain in the sample is due to applying stress on the sample. The microstrain plot revealed that the obtained microstrain is compressive in nature, which may be due to the incorporation of Cu^{2+} and Mg^{2+} ions in the adsorbent.

3.2. Morphological Analysis. Figure 3(a) reveals the surface characteristics of the pristine spinel ferrite. Figure 3(b) reveals the surface characteristics of the silica-coated ferrite. Both pristine and silica-decorated samples exhibited spherical particle shapes. The degree of agglomeration among the nanoparticles was relatively high in the pristine ferrite sample due to the existence of magnetic dipole−dipole interactions. The agglomeration among the nanoparticles of silica-decorated ferrite is somewhat lower than the pristine ferrite. A decrease in agglomeration is due to increased dispersion and reduced magnetic affinity among the nanoparticles due to the silica

https://doi.org/10.1021/acsomega.3c05764
ACS Omega 2023, 8, 47623−47634

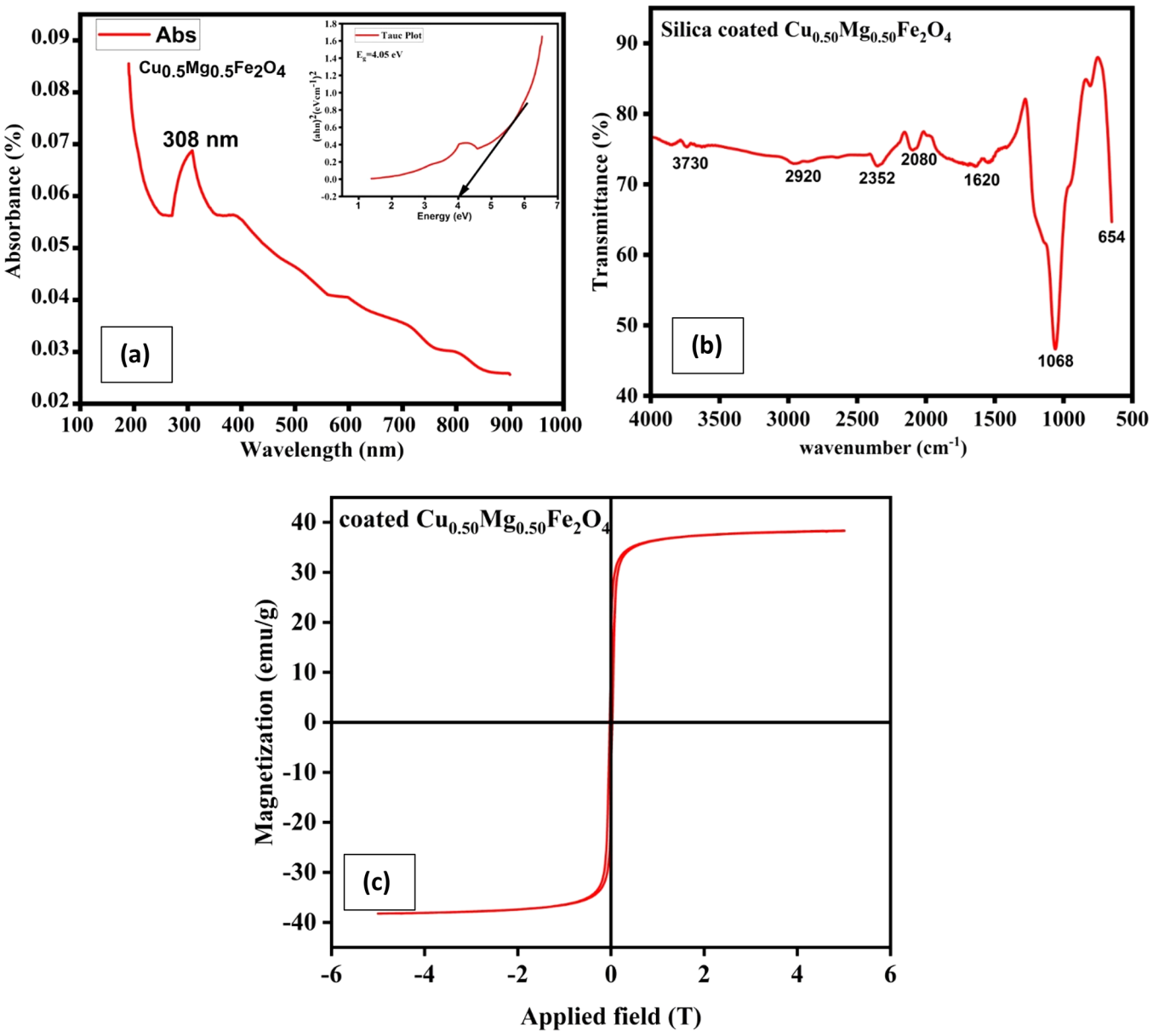

Figure 4. (a) UV−vis spectrum with Tauc plot, (b) FTIR spectrum, and (c) hysteresis loop of the silica-coated $Cu_{0.50}Mg_{0.50}Fe_2O_4$ adsorbent.

barrier. The particle size distribution was fine in both samples, confirming the controlled growth and coating of adsorbent nanoparticles.[31] The surface morphology of silica-decorated ferrite nanoparticles was rougher than that of pristine ferrite nanoparticles. The structures formed on the superficial layer of the samples were not destroyed or fractured, and well-shaped particles were obtained due to silica coating. Similar surfaces for silica-coated ferrites have already been reported by Ghalehno et al.[32] Moreover, very clear particle boundaries were demonstrated by silica-coated ferrite with a reduced particle size compared to pristine ferrite. The silica coating improved the surface-to-volume ratio, corrosion resistance and stability of nanoparticles.[33]

The internal morphology and lattice fringes were observed from the TEM images in Figure 3(c). The crystallite size, estimated from XRD, differs from the particle size calculated through microscopic analysis. According to the preparation techniques, one particle may include many crystallites. XRD analyzes the size of the small domains within the grains. TEM analysis reveals better crystallinity of the nanoparticles. The image of Figure 3(c) shows the high-resolution TEM images of the nanoparticle, clearly showing the patterns of lattice fringes in the nanoparticles. The prominent lattice fringes with 0.248 nm interplanar spacing correlate well with (311) crystal plane of the cubic spinel structure.[34] TEM images showed the predictable orientation of lattice fringes by suggesting a better crystallinity of the structures.

3.3. Optical and Magnetic Characteristics. UV−vis spectroscopy is not typically a primary method of characterizing the adsorption characteristics of spinel ferrite adsorbents. However, this technique can provide insights into the electronic structures of such adsorbents. By measuring the absorption of UV or visible light by a material, it is possible to determine the energy levels and electronic transitions within the material. This information can be important for understanding how the molecules or ions of the adsorbate interact with the adsorbent surface. Since $Cu_{0.5}Mg_{0.5}Fe_2O_4$ is a mixed metal ferrite compound, its electronic transitions involve the

https://doi.org/10.1021/acsomega.3c05764
ACS Omega 2023, 8, 47623−47634

movement of electrons between energy levels associated with different elements within the compound. The major electronic transitions in $Cu_{0.50}Mg_{0.50}Fe_2O_4$ involve 3d orbitals of Fe ions.[35] These ions undergo electronic transitions between various 3d orbitals. The oxidation state of Fe ions can influence these transitions, the coordination environment of Fe ions, and crystal field splitting. The electronic transitions involving Cu and Mg ions may occur in different energy ranges and may not be as prominent as the Fe ion transitions. Cu, Mg, and Fe ions in $Cu_{0.5}Mg_{0.5}Fe_2O_4$ can lead to charge transfer transitions between these elements. Electronic transitions across the bandgap can also occur from the valence band of the nanoparticle material to the conduction band. The bandgap of the material determines the energy of these transitions.

The bandgap of silica-coated $Cu_{0.5}Mg_{0.5}Fe_2O_4$ was studied by UV−vis spectroscopy in the range 200−900 nm. About 15 mL of deionized water was used to dissolve 3 mg of prepared sample and sonicated for 30 min. After this, the solution was examined by a UV−vis spectroscopic analysis. The UV−vis of coated $Cu_{0.5}Mg_{0.5}Fe_2O_4$ in Figure 4(a) showed an absorbance peak at 308 nm, indicating the creation of $Cu_{0.5}Mg_{0.5}Fe_2O_4$ and electronic transitions between 3d orbits. The Cu and Mg ions in the adsorbent create surface defects and cause a wide bandgap; therefore, the light absorption by the adsorbent was slightly toward UV range due to the larger ionic radii of both metals. Band gap energy (E_g) was determined from the absorbance curve by utilizing the Tauc relation in eq 6. The inset of Figure 4(a) reports a Tauc plot of the modified ferrite nanoparticles.

$$(\alpha h\nu)n = K(h\nu - E_g)^{1/2} \tag{6}$$

where α demonstrates the optical absorption coefficient. In semiconductors, n is a transition type, which can have various values (2, 3, 1/2, 1/3), and K is the constant known as the band tailing parameter. Meanwhile, ν is the frequency of incident photons, and h is Planck's constant. The values of n, related to the material, have been specified as 2, 1/2, 3, and 3/2, corresponding to tolerable indirect, direct, forbidden indirect, and forbidden direct transitions.[36] It is worth noting that the sort of band gap corresponding to silica-coated $CuMgFe_2O_4$ is still up for debate. Few researchers recommended that the band gap is indirect, and few suggested their band gap is direct.[37] The latest analysis of the electrical structure of $CuMgFe_2O_4$ confirmed the occurrence of a direct band gap. As a result, the direct band gap for $CuMgFe_2O_4$ is chosen and n = 1/2 is considered.

FTIR analysis was performed in the range 500−4000 cm^{-1} to determine the various functional groups in silica-coated ferrite, as shown in Figure 4(b). A very bulbous peak at 654 cm^{-1} indicated Fe−O bond vibrations, a characteristic feature of ferrites.[38] The sharp peak appeared at 1068 cm^{-1}, indicating dipole−induced dipole interaction between silica and ferrite ceramic.[39] A band at 1620 cm^{-1}, demonstrating H−O−H bending vibrations, appeared due to water molecules present in the silica-coated spinel ferrite and a band witnessed at 1680 cm^{-1} revealed OH stretching associated with hydrogen bonding, which arises from manganite.[40] Relatively weak vibration bands at 2352 and 2920 cm^{-1} were referred to CO_2 and C−H stretching vibrations.[41]

Measurement of the magnetic properties of materials is commonly accomplished by performing VSM analysis. Figure 4(c) reports a typical hysteresis loop of the adsorbent at room temperature. The remnant magnetization, saturation magnetization, and coercivity can be determined from the hysteresis loop. The synthesized silica-coated spinel ferrite exhibited saturation magnetization at 37.80 emu/g, remnant magnetization at 20.87 emu/g, and coercivity at 0.03 T. A slight decline in saturation magnetization was observed for silica-coated ferrite compared to pristine ferrite. Silica coating generates a nonmagnetic sheet on ferrite particles, which disrupts the exchange interactions between spins. Another important factor is surface oxidation produced due to silica coating, which significantly reduces the magnetic moment as compared to that of pristine ferrites. It consequently causes a decline in saturation magnetization.[42,43] The squareness ratio was calculated at 0.55, which is greater than 0.5, demonstrating the development of single magnetic domain structure in the ferrite adsorbent.[43]

3.4. Adsorption Mechanism of Silica-Coated Adsorbent. The adsorption of heavy metal ions on silica-coated $CuMgFe_2O_4$ adsorbent involves the structural properties of the adsorbent, properties of adsorbate, and adsorption conditions. So, the adsorption of metal ions involves chemical and physical processes. The morphological analyses of adsorbent nanoparticles revealed spherical shape and narrow size distribution. TEM analysis reveals better crystallinity of the nanoparticles. The prominent lattice fringes with 0.248 nm interplanar spacing correlate well with the (311) crystal plane of the cubic spinel structure.[34] TEM images showed the predictable orientation of lattice fringes by suggesting the crystallinity of the structures. These findings suggest that a large active surface area is available for the interaction of adsorbate metal ions with the surface and, consequently, the increased adsorption capacity. Heavy metal ions are normally positively charged, whereas the surface of silica-coated $CuMgFe_2O_4$ adsorbent is negatively charged. Adsorption of adsorbate ions onto the adsorbent surface is caused by electrostatic attraction. The tested adsorbent under examination may also have some active sites with exchangeable hydroxyl groups. Through the ion exchange mechanism, metal ions replace these exchangeable groups, resulting in their adsorption onto the adsorbent. The other factors involved in the adsorption of heavy metal ions onto the adsorbent are complexation adsorption isotherms and solution pH. Silanol (−SiOH) and other hydroxyl functional groups on the absorbent surface form complexes with metal ions to immobilize these metal ions on the adsorbent nanoparticles. The Langmuir and Freundlich isotherms are also used to get insights into the affinity and adsorption capacity of adsorbents for selected heavy metal ions. Therefore, both adsorption isotherms were studied to deduce an effective adsorption mechanism of the tested silica-coated $CuMgFe_2O_4$ adsorbent.

3.5. Adsorption Kinetics. To understand the adsorption process, pseudo-models were adopted to study the behavior of the adsorbent. As a reversible process, pseudo-first-order kinetics was employed instead of physisorption in this reversible process, where equilibrium is maintained between liquid and solid. An interpretation of the pseudo-second-order kinetic model can explain how heavy metal ions adsorb onto adsorbents during the adsorption process. Hazardous metal ions interact chemically with the surface of silica-coated adsorbents to affect their cation exchange capacity. It is widely admitted that the pseudo-first-order kinetic model is one of the most useful models for studying the process of adsorption on solid surfaces. Typically, the pseudo-first-order model fits the

https://doi.org/10.1021/acsomega.3c05764
ACS Omega 2023, 8, 47623−47634

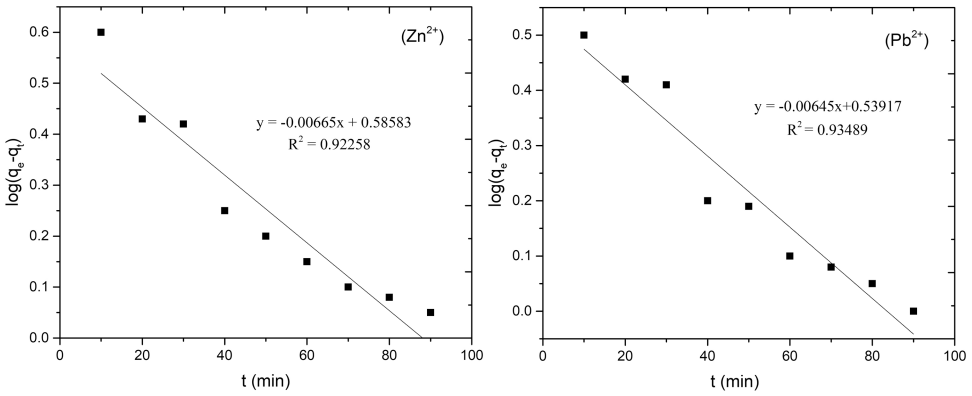

Figure 5. Adsorption of Zn^{2+} and Pb^{2+} ions onto silica-coated $CuMgFe_2O_4$ adsorbent for pseudo-first-order kinetics.

Table 1. Comparison of the Findings of Kinetic Adsorption Models for Different Reported Adsorbents

		pseudo-1st-order model			pseudo-2nd-order model			
adsorbent type	heavy metals	q_e (mg/g)	k_1 (1/min)	R^2	q_e (mg/g)	k_2	R^2	ref
$CoFe_2O_4$@SiO_2−NH_2 NPs	Cu(II)				177.8	0.000401	0.99897	[47]
	Pb(II)				181.6	0.000453	0.99997	
Dioctylphthalate triethylenetetraamine (DOP-TETA) MNPs	Zn(II)	13.89	0.01	0.81	43.1	0.00273	0.99	[48]
Lemon wood Biochar	Zn(II)	52.19	0.055	0.986	100	0.002	0.999	[49]
	Cu(II)	54.43	0.049	0.985	111.1	0.0016	0.99	
Chitosan functionalized Fe_3O_4 NPs	Pb(II)	112.4	0.03928	0.9624	152.8	0.0002	0.9613	[50]
SPIONs/gel	Cu(II)	18.834	0.055	0.992	20.779	0.004	0.991	[51]
	Zn(II)	14.109	0.137	0.986	14.888	0.019	0.998	
ZnO NPs	Pb(II)	5.8	0.014	0.959	4.5	0.048	0.997	[52]
$Cu_{0.50}Mg_{0.50}Fe_2O_4$@$SiO_2$	Pb(II)	3.46	0.0148	0.9349	37.13	0.00189	0.9826	This study
	Zn(II)	3.8532	0.0153	0.9226	34.65	−0.0058	0.9868	

kinetics of adsorption, occurring via diffusion through an interface.[44] To express the pseudo-first-order model in a linear form, we can follow eq 7:

$$\frac{dq_t}{dt} = k_1(q_e - q_t) \tag{7}$$

In this model, q_t indicates the quantity adsorbed at t time and q_e is the quantity adsorbed at the equilibrium stage, while k_1 represents the pseudo-first-order constant. Equation 7 gets the following form (eq 8) after applying boundary conditions.

$$\ln(q_e - q_t) = \ln(q_e) - \frac{K1}{2.303}t \tag{8}$$

Using the linear graphs of the logarithms of q_e and q_t over a period of time, one can determine the value of k_1. An adsorption process obeying pseudo-first-order kinetics will have $\log(q_e - q_t)$ as the intercept against the $\log(q_e)$ plot. It is extremely difficult to determine the precise value of q_e for slow adsorption because equilibrium condition are difficult to achieve.[45] Magnetic ferrite nanoparticles absorbed Zn^{2+} and Pb^{2+} ions content of 3.85 and 3.46 mg/g, respectively, at the equilibrium state. Figure 5 shows plots of Zn^{2+} and Pb^{2+} ion adsorption onto the silica-coated $CuMgFe_2O_4$ nanoparticles based on a pseudo-first-order model. Table 1 reports the estimated kinetic factors. R^2 values reported in previous research works ranged from 0.92 to 0.99 for heavy metals Pb(II), Cd(II), and Zn^{2+} elimination using different additives in ferrites.[15] The obtained values of kinetic parameters for silica-coated $CuMgFe_2O_4$ in the current study were slightly lower than reported for $NiFe_2O_4$, and $CoFe_2O_4$, indicating that the reaction kinetics of reported materials are more precisely described through pseudo-first-order kinetic model.[46]

Pseudo-second-order kinetics forecasts the adsorption response during the adsorption procedure because chemisorption is a rate-limiting phase. The rate of the reaction can be calculated as a function of the product of the concentrations of the reactants assuming that the reaction occurs according to a second-order rate law. When contrasting the pseudo-first-order model, this model can be used to determine equilibrium adsorption capacity, eliminating the need to perform experiments to measure equilibrium adsorption capability.[53] The differential expression for pseudo-second-order kinetics is given in eq 9.

$$\frac{dq_t}{dt} = k_2(q_e - q_t)^2 \tag{9}$$

A pseudo-second-order kinetic model is established after the boundary condition has been considered and mathematically developed as

$$t/q_t = 1/k(q_e)^2 + t/q_e \tag{10}$$

$$Z = K_2 q_e^{\ 2} \tag{11}$$

In the above relation, Z represents the initial adsorption rate, q_e demonstrates the equilibrium amount of the heavy metals, and K_2 reveals the pseudo-second-order rate parameter. Plotting t/q_t against t reveals a direct relationship, which can be used to estimate the amount of adsorbed adsorbate at equilibrium. A

https://doi.org/10.1021/acsomega.3c05764
ACS Omega 2023, 8, 47623−47634

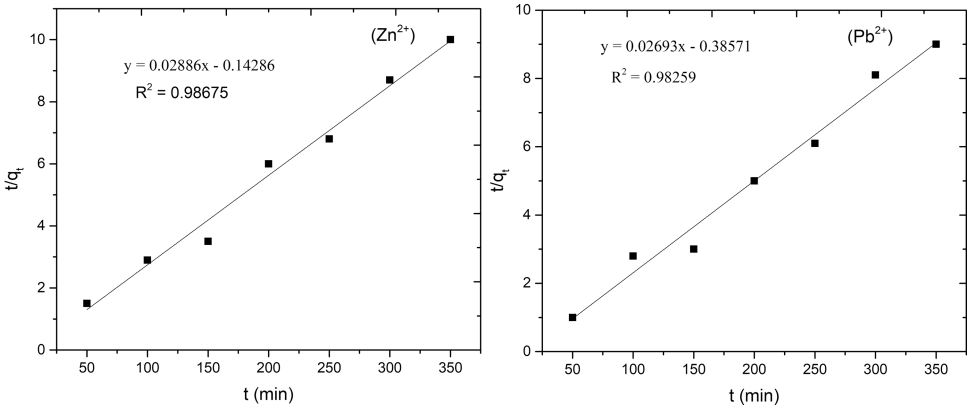

Figure 6. Adsorption of Zn^{2+} and Pb^{2+} ions onto silica-coated $CuMgFe_2O_4$ adsorbent for pseudo-second-order kinetics.

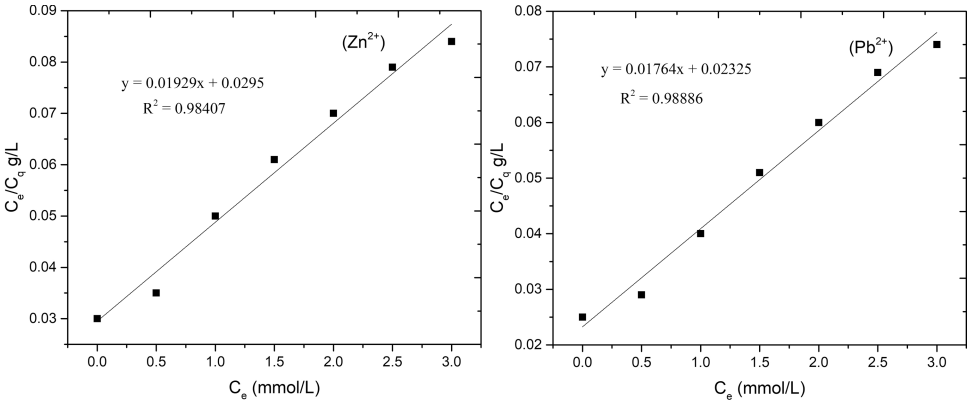

Figure 7. Langmuir adsorption isotherm plots for adsorption of Zn^{2+} and Pb^{2+} onto the $CuMgFe_2O_4$ adsorbent.

Table 2. Comparison of Adsorption of Different Adsorbents Based on Isotherm Models

		Freundlich isotherm model			Langmuir isotherm model			
adsorbent type	heavy metals	n	K_f (mg/g)	R^2	q_{max}	K_L (L/mg)	R^2	ref
Dioctylphthalate triethylenetetraamine (DOP-TETA) MNPs	Zn(II)	0.57	5.58	0.9	23.75	0.44	0.93	[48]
Fe_3O_4@SiO_2−NH_2 NPs	Zn(II)	1.6471	9.9115	0.9923	169.492	36.76	0.8094	[57]
Chitosan functionalized Fe_3O_4 NPs	Pb(II)	2.6716	2.369	0.9764	95.36		0.9881	[50]
Magnetite-NH_2 NPs	Cu(II)	1.79	5.81	0.972	28.7	0.25	0.996	[58]
ZnO NPs	Pb(II)	2.81	3.16	0.914	19.65	0.0839	0.999	[52]
SPIONs/gel/PVA	Cu(II)	2.2867	45.658	0.976	56.051	3.397	0.993	[51]
	Zn(II)	2.2732	32.866	0.979	40.865	3.267	0.999	
Chitosan based Fe_3O_4 NCs	Cu(II)				21.5	0.0165	0.9932	[58]
Lemon wood biochar	Zn(II)	4.41	49.77	0.91	100	0.27	0.998	[49]
	Cu(II)	4.06	56.1	0.975	111.1	1	0.999	
$Cu_{0.50}Mg_{0.50}Fe_2O_4$@$SiO_2$	Pb(II)	1.2	25.66	0.939	56.689	0.75	0.98886	This study
	Zn(II)	1.16	32.57	0.96314	51.84	0.654	0.98407	

pseudo-second-order kinetic model for Pb^{2+} and Zn^{2+} ions is demonstrated in Figure 6 as a plot of its linearized form. The adsorption rate constants are compared with those in the published literature in Table 1. For the adsorption by synthesized silica-coated spinel ferrite toward Zn^{2+} and Pb^{2+} ions, correlation coefficient R^2 of the pseudo-second-order kinetic model was observed much greater than the pseudo-first-order kinetic model. It shows that the pseudo-second-order kinetic model is a better fit than the pseudo-first-order kinetic model. The obtained values of kinetic parameters also agreed with the reported values of the pseudo-second-order kinetic model for ferric oxide adsorbent.[54]

3.6. Adsorption Isotherms. Freundlich and Langmuir's isotherms were utilized to investigate the adsorption capability of silica-coated $CuMgFe_2O_4$. The association between the adsorbent and the adsorbate was represented to better understand the phenomenon. An adsorbent's maximum capacity for adsorbing adsorbate can be determined by its adsorption isotherms. Temperature, pressure, and concentration can be applied to calculate the adsorbent−adsorbate behavior using isotherms. In adsorption procedures, such as those used to remove contaminants from wastewater or separate gases, the Langmuir isotherm is commonly used for design and optimization. Langmuir's model provides an initial

https://doi.org/10.1021/acsomega.3c05764
ACS Omega 2023, 8, 47623−47634

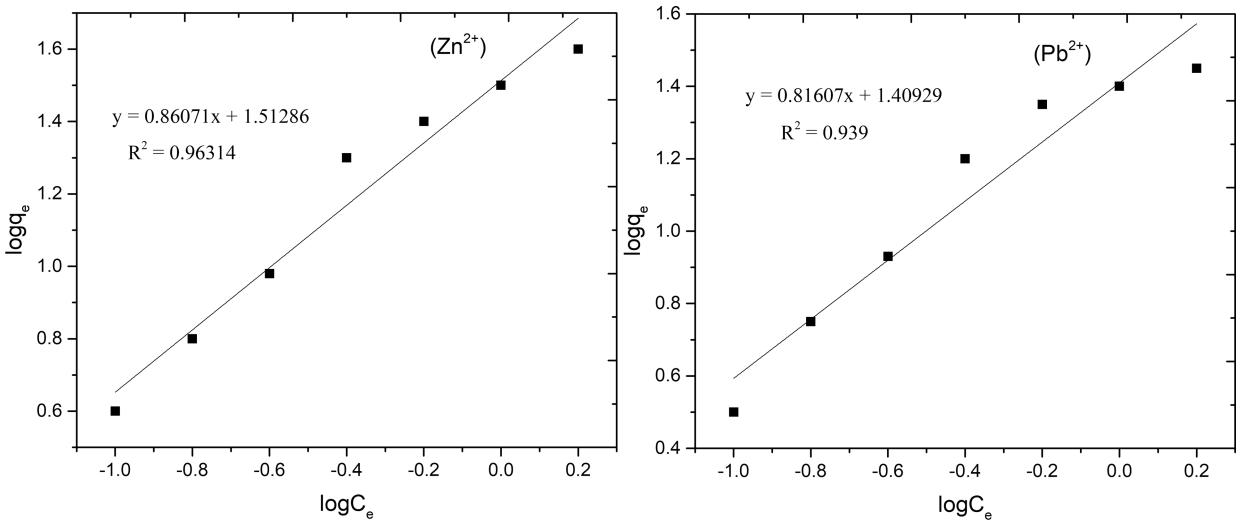

Figure 8. Freundlich plots for adsorption of Zn^{2+} and Pb^{2+} ions onto the silica-coated $CuMgFe_2O_4$ adsorbent.

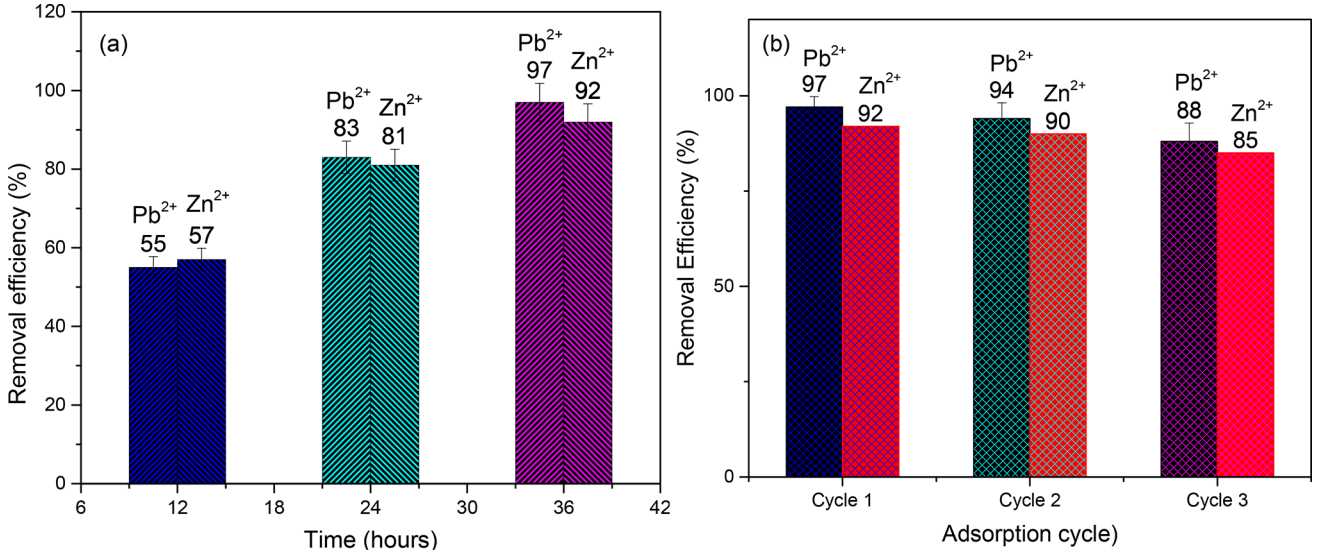

Figure 9. (a) Removal efficiency of silica-coated $CuMgFe_2O_4$ for Pb^{2+} and Zn^{2+} ions, and (b) stability test of silica-coated $CuMgFe_2O_4$ for Pb^{2+} and Zn^{2+} ions over three cycles.

approach for quantifying and comparing gas adsorption on solid surfaces.[55] At equilibrium, the adsorption and desorption rates of adsorbate are equal in the adsorption process. Multilayer formation and partial mobility and differences in molecular sizes are not considered in Langmuir's model. Langmuir's model of adsorption equilibrium describes the equilibrium between solids and solutions as explained in eq 12.

$$q_e = \frac{q_{max} K_L C_e}{1 + K_L C_e} \quad (12)$$

In the above equation, q_e reveals the solute quantity consumed per unit mass of adsorbent when equilibrium is established. C_e demonstrates the concentration of the solute at an equilibrium state. In addition, q_{max} shows the maximum adsorption capability of the adsorbent and K_L represents the equilibrium constant. The fitting curves for Langmuir isotherms are presented in Figure 7 while the parameters obtained from these curves are compared with the published literature in Table 2. Since the Langmuir model has very large R^2 values for both Zn^{2+} and Pb^{2+} ions, the adsorption process can be explained accurately with this method. Similar values of reaction parameters were witnessed for different ferrites, including $ZnFe_2O_4$, $NiFe_2O_4$, and iron oxide adsorbents, demonstrating the effectiveness of the Langmuir kinetic model for investigating reaction kinetics.[56]

The Freundlich isotherm is frequently applied as an empirical equation formulated from experimental data because it depicts the adsorption process of organic pollutants and heavy metal ions on different adsorbents. Herbert Freundlich proposed the model as an addition to Henry's model in 1906.[59] To develop Freundlich isotherms for adsorbents, it was necessary to develop a heterogeneous surface consisting of many adsorption sites. When the adsorption energy decreases exponentially at the end of the adsorption phase, the amount adsorbed is the sum of the adsorption rates on all sites. It has the advantage of being used for multilayer adsorption; thus, Freundlich kinetics can be seen as more advantageous than Langmuir kinetics. When chemisorption is predominant in the adsorption process of monolayers, Freundlich's model explains

https://doi.org/10.1021/acsomega.3c05764
ACS Omega 2023, 8, 47623−47634

the monolayer adsorption process. Freundlich model can be expressed mathematically in eq 13.

$$\log q_e = (\log C_e)/n + \log K_F \quad (13)$$

In the above equation, C_e reveals the equilibrium concentration, while q_e shows the amount of metal ions adsorbed onto an adsorbent, K_F denotes the Freundlich constant, and n shows the intensity of adsorption. Furthermore, the estimated values of n for adsorption of Zn^{2+} and Pb^{2+} ions are greater than unity. Figure 8 shows Freundlich plots for the adsorption of Zn^{2+} and Pb^{2+} ions onto silica-coated $CuMgFe_2O_4$. R^2 values for Zn^{2+} and Pb^{2+} ions revealed an important relationship between the variables in the Freundlich model. According to Table 2, Freundlich isotherm parameters for both Zn^{2+} and Pb^{2+} ions revealed lower correlation coefficients for the Freundlich isotherm than the Langmuir Isotherm model.

No leaching of Cu ions from $CuMgFe_2O_4$ into the aqueous solution was observed in this study since this adsorbent is generally stable in neutral or slightly basic environments. However, in acidic environments, the solubility of copper ions (Cu^{2+}) may increase, potentially leading to leaching. The other ions in the solution can also affect the Cu leaching. These ions may form a complex with Cu ions to reduce their solubility and leaching. Since Zn^{2+} and Pb^{2+} ions are generally neutral, they do not alter the neutrality of the aqueous solution under moderate concentrations. A coating on the adsorbent nanoparticles may also create a barrier between the adsorbent and the surrounding environment. The silica coating of the adsorbent therefore also prevented the leaching of constituent ions from the adsorbent.

3.7. Removal Efficiency. The Zn^{2+} and Pb^{2+} ion removal efficiency of silica-coated $CuMgFe_2O_4$ was estimated over different times and cycles. The Pb^{2+} and Zn^{2+} removal capability of the adsorbent from wastewater was estimated by measuring initial and final amounts of ions in water by applying eq 14.

$$R\ \% = [(C_0 - C_e)/C_0] \times 100 \quad (14)$$

Removal efficiencies of silica-coated $CuMgFe_2O_4$ for Pb^{2+} and Zn^{2+} ions were measured at about 97% and 92%, respectively, after 36 h of adsorption time. The removal efficiency for Pb^{2+} ions is notably higher than that for Zn^{2+} ions, as shown in Figure 9(a). The tested adsorbent also showed good stability over repeated adsorption cycles, as revealed in Figure 9(b). The efficiency for Pb^{2+} ion adsorption decreased from 97% to 88% after three consecutive adsorption cycles. Similarly, the adsorption efficiency for Zn^{2+} ions decreased from 92% to 85% after three consecutive adsorption cycles.

4. CONCLUSIONS

A silica-coated $CuMgFe_2O_4$ adsorbent was synthesized and examined for the treatment of the Zn^{2+} and Pb^{2+} pollutants. The silica modified adsorbent showed excellent adsorption properties, stability, and good magnetic characteristics. XRD and FTIR investigations endorsed the successful formation of spinel ferrites. SEM analysis demonstrated narrow distribution of particle size with reduced agglomeration in silica-decorated ferrites. Optical characteristics analysis demonstrated that silica coating enhanced the energy band gap up to 4 eV. Magnetic analysis revealed saturation magnetization and remnant magnetization at 37.80 and 20.87 emu/g, respectively. The adsorption kinetics study validated that the pseudo-second-order model is the best fit, while the isotherm analysis demonstrated that the Langmuir fit was good throughout the board. The synthesized ferrites can separate when an external magnetic field is applied so they can be used for multiple cycles. Synthesized silica-coated $CuMgFe_2O_4$ demonstrated an excellent removal efficiency for Zn^{2+} and Pb^{2+} ions. The adsorbent revealed 92% and 97% removal efficiencies for Zn^{2+} and Pb^{2+} ions, respectively. The adsorption efficiency of the adsorbent decreased from 97% to 88% for Pb^{2+} ions and 92% to 85% for Zn^{2+} ions after three consecutive adsorption cycles. These findings suggest reasonably good stability of the tested adsorbent.

■ ASSOCIATED CONTENT

Data Availability Statement

The available data has been included in this paper in the form of images, figures and tables. There is no additional data to report as a separate file.

■ AUTHOR INFORMATION

Corresponding Author

Muhammad Yasin Naz − *Department of Physics, University of Agriculture Faisalabad, 38040 Faisalabad, Pakistan;* orcid.org/0000-0002-8490-7819; Email: yasin306@uaf.edu.pk

Authors

Muhammad Irfan − *Electrical Engineering Department; College of Engineering, Najran University Saudi Arabia, Najran 61441, Saudi Arabia;* orcid.org/0000-0003-4161-6875

Anam Arif − *Department of Physics, University of Agriculture Faisalabad, 38040 Faisalabad, Pakistan*

Muhammad Adnan Munir − *Department of Physics, University of Agriculture Faisalabad, 38040 Faisalabad, Pakistan*

Shazia Shukrullah − *Department of Physics, University of Agriculture Faisalabad, 38040 Faisalabad, Pakistan;* orcid.org/0000-0002-4474-3768

Saifur Rahman − *Electrical Engineering Department; College of Engineering, Najran University Saudi Arabia, Najran 61441, Saudi Arabia*

Mohammed Jalalah − *Electrical Engineering Department; College of Engineering, Najran University Saudi Arabia, Najran 61441, Saudi Arabia*

Abdulkarem H. M. Almawgani − *Electrical Engineering Department; College of Engineering, Najran University Saudi Arabia, Najran 61441, Saudi Arabia*

Complete contact information is available at: https://pubs.acs.org/10.1021/acsomega.3c05764

Notes

The authors declare no competing financial interest.

■ ACKNOWLEDGMENTS

The authors would like to acknowledge the support of the Deputy for Research and Innovation - Ministry of Education, Kingdom of Saudi Arabia for this research through a grant (NU/IFC/2/SERC/-/17) under the Institutional Funding Committee at Najran University, Kingdom of Saudi Arabia.

https://doi.org/10.1021/acsomega.3c05764
ACS Omega 2023, 8, 47623−47634

REFERENCES

(1) Rasheed, T.; Shafi, S.; Bilal, M.; Hussain, T.; Sher, F.; Rizwan, K. Surfactants-based remediation as an effective approach for removal of environmental pollutants—A review. *J. Mol. Liq.* **2020**, *318*, 113960.

(2) Li, Y.; Bai, P.; Yan, Y.; Yan, W.; Shi, W.; Xu, R. Removal of Zn^{2+}, Pb^{2+}, Cd^{2+}, and Cu^{2+} from aqueous solution by synthetic clinoptilolite. *Microporous Mesoporous Mater.* **2019**, *273*, 203−211.

(3) Mitra, S.; Chakraborty, A. J.; Tareq, A. M.; Emran, T. B.; Nainu, F.; Khusro, A.; Idris, A. M.; Khandaker, M. U.; Osman, H.; Alhumaydhi, F. A. Impact of heavy metals on the environment and human health: Novel therapeutic insights to counter the toxicity. *Journal of King Saud University-Science* **2022**, *34*, 101865.

(4) Liosis, C.; Papadopoulou, A.; Karvelas, E.; Karakasidis, T. E.; Sarris, I. E. Heavy Metal Adsorption Using Magnetic Nanoparticles for Water Purification: A Critical Review. *Materials* **2021**, *14* (24), 7500.

(5) Ahmed, M. J.; Hameed, B. H.; Hummadi, E. H. Review on recent progress in chitosan/chitin-carbonaceous material composites for the adsorption of water pollutants. *Carbohydr. Polym.* **2020**, *247*, 116690.

(6) Barakat, M. A. New trends in removing heavy metals from industrial wastewater. *Arabian Journal of Chemistry* **2011**, *4* (4), 361−377.

(7) Fu, F.; Wang, Q. Removal of heavy metal ions from wastewaters: A review. *Journal of Environmental Management* **2011**, *92* (3), 407−418.

(8) Sarkar, A.; Paul, B. The global menace of arsenic and its conventional remediation - A critical review. *Chemosphere* **2016**, *158*, 37−49.

(9) Sun, J.; Liu, L.; Yang, F. A WO_3/PPy/ACF modified electrode in electrochemical system for simultaneous removal of heavy metal ion Cu2+ and organic acid. *Journal of Hazardous Materials* **2020**, *394*, 122534.

(10) Wan Nafi, A.; Taseidifar, M. Removal of hazardous ions from aqueous solutions: Current methods, with a focus on green ion flotation. *Journal of Environmental Management* **2022**, *319*, 115666.

(11) Liao, Z.l.; Zhao, Z. C.; Zhu, J. C.; Chen, H.; Meng, D. Z. Complexing characteristics between Cu(II) ions and dissolved organic matter in combined sewer overflows: Implications for the removal of heavy metals by enhanced coagulation. *Chemosphere* **2021**, *265*, 129023.

(12) Hutton-Ashkenny, M.; Ibana, D.; Barnard, K. R. Reagent selection for recovery of nickel and cobalt from nitric acid nickel laterite leach solutions by solvent extraction. *Minerals Engineering* **2015**, *77*, 42−51.

(13) Gupta, K.; Joshi, P.; Gusain, R.; Khatri, O. P. Recent advances in adsorptive removal of heavy metal and metalloid ions by metal oxide-based nanomaterials. *Coord. Chem. Rev.* **2021**, *445*, 214100.

(14) Tan, T. H.; Mo, K. H.; Ling, T. C.; Lai, S. H. Current development of geopolymer as alternative adsorbent for heavy metal removal. *Environmental Technology & Innovation* **2020**, *18*, 100684.

(15) Wadhawan, S.; Jain, A.; Nayyar, J.; Mehta, S. K. Role of nanomaterials as adsorbents in heavy metal ion removal from waste water: A review. *Journal of Water Process Engineering* **2020**, *33*, 101038.

(16) Ahmad Wani, A.; Shahadat, M.; Wazed Ali, S.; Ziauddin Ahammad, S.; Kashif Uddin, M. Recent advances and future perspectives of polymer-based magnetic nanomaterials for detection and removal of radionuclides: a review. *J. Mol. Liq.* **2022**, *365*, 119976.

(17) Mokkarat, A.; Kruanetr, S.; Sakee, U. One-step continuous flow synthesis of aminopropyl silica-coated magnetite nanoparticles. *Journal of Saudi Chemical Society* **2022**, *26* (4), 101506.

(18) Huang, J. H.; Dong, J.; Liu, Z. L.; Liu, Y. P.; Wu, D. Y. Degradation of Dyes by H2O2 with Activated Charcoal Supported $MgFe_2O_4$ under Microwave Irradiation. *Advanced Materials Research* **2014**, *1004-1005*, 972−977.

(19) Naz, M. Y.; Irfan, M.; Shukrullah, S.; Ahmad, I.; Ghuffar, A.; Niazi, U. M.; Rahman, S.; Jalalah, M. S.; Alsaiari, M. A.; Khan, M. K. A. Study of structural, magnetic and optical properties of oxygen plasma-treated manganese-doped iron oxide photocatalyst for wastewater treatment. *Appl. Phys. A: Mater. Sci. Process.* **2021**, *127* (7), 491.

(20) Tang, W.; Su, Y.; Li, Q.; Gao, S.; Shang, J. K. Superparamagnetic magnesium ferrite nanoadsorbent for effective arsenic (III, V) removal and easy magnetic separation. *Water Res.* **2013**, *47* (11), 3624−3634.

(21) Shukrullah, S.; Naz, M. Y.; Mohamed, N. M.; Ibrahim, K. A.; AbdEl-Salam, N. M.; Ghaffar, A. CVD synthesis, functionalization and CO_2 adsorption attributes of multiwalled carbon nanotubes. *Processes* **2019**, *7* (9), 634.

(22) Qiao, K.; Tian, W.; Bai, J.; Wang, L.; Zhao, J.; Du, Z.; Gong, X. Application of magnetic adsorbents based on iron oxide nanoparticles for oil spill remediation: A review. *Journal of the Taiwan Institute of Chemical Engineers* **2019**, *97*, 227−236.

(23) Rezlescu, E.; Rezlescu, N.; Popa, P. D. Fine-grained MgCu ferrite with ionic substitutions used as humidity sensor. *J. Magn. Magn. Mater.* **2005**, *290*, 1001−1004.

(24) Rezlescu, E.; Rezlescu, N.; Tudorache, F.; Popa, P. D. Effects of replacing Fe by La or Ga in Mg0. 5Cu0. 5Fe2O4. Humidity sensitivity. *J. Magn. Magn. Mater.* **2004**, *272*, E1821−E1822.

(25) Nadeem, K.; Ali, L.; Gul, I.; Rizwan, S.; Mumtaz, M. Effect of silica coating on the structural, dielectric, and magnetic properties of maghemite nanoparticles. *J. Non-Cryst. Solids* **2014**, *404*, 72−77.

(26) Leal, E.; Dantas, J.; dos Santos, P. T. A.; Bicalho, S. M. d. C. M.; Kiminami, R. H. G. A.; da Silva, M. R.; de Melo Costa, A. C. F. Effect of the surface treatment on the structural, morphological, magnetic and biological properties of MFe_2O_4 iron spinels (M= Cu, Ni, Co, Mn and Fe). *Appl. Surf. Sci.* **2018**, *455*, 635−645.

(27) Ferrer, C.; Isasi, J.; Arévalo, P.; Fernández-Ramos, M.; Rapp, M.; Alcolea, M.; Marco, J. F.; Martín-Hernández, F. Structural and magnetic studies of $NiFe_2O_4$ and $NiFe_2O_4$@ SiO_2-Silane agent samples useful for the removal of Cu^{2+} ions. *J. Alloys Compd.* **2022**, *899*, 163403.

(28) Ibrahim, I.; Ali, I. O.; Salama, T. M.; Bahgat, A. A.; Mohamed, M. M. Synthesis of magnetically recyclable spinel ferrite (MFe_2O_4, M= Zn, Co, Mn) nanocrystals engineered by sol gel-hydrothermal technology: High catalytic performances for nitroarenes reduction. *Applied Catalysis B: Environmental* **2016**, *181*, 389−402.

(29) Zeb, F.; Qureshi, A. R.; Nadeem, K.; Mumtaz, M.; Krenn, H. Surface effects in uncoated and amorphous SiO_2 coated cobalt ferrite nanoparticles. *J. Non-Cryst. Solids* **2016**, *435*, 69−75.

(30) Saleem, S.; Irfan, M.; Naz, M. Y.; Shukrullah, S.; Munir, M. A.; Ayyaz, M.; Alwadie, A. S.; Legutko, S.; Petrů, J.; Rahman, S. Investigating the Impact of Cu^{2+} Doping on the Morphological, Structural, Optical, and Electrical Properties of $CoFe_2O_4$ Nanoparticles for Use in Electrical Devices. *Materials* **2022**, *15* (10), 3502.

(31) Munir, M. A.; Naz, M. Y.; Shukrullah, S.; Ansar, M. T.; Abbas, G.; Makhlouf, M. M. Microwave plasma treatment of NiCuZn ferrite nanoparticles: a novel approach of improving opto-physical and magnetic properties. *Appl. Phys. A: Mater. Sci. Process.* **2022**, *128* (4), 345.

(32) Ghalehno, M. H.; Parvizi, A.; Mirzaei, M. A novel electrochemical sensor for the determination of diphenylhydramine hydrochloride based on a carbon paste electrode (CPE) modified with ferrite-cobalt-silica/ionic liquid nanocomposite. *Russian Journal of Electrochemistry* **2022**, *58* (5), 381−390.

(33) Patil, S.; Tandon, R.; Tandon, N. A current research on silica coated ferrite nanoparticle and their application. *Current Research in Green and Sustainable Chemistry* **2021**, *4*, 100063.

(34) Zhang, S.; Xu, Y.; Zhao, D.; Chen, W.; Li, H.; Hou, C. Preparation of Magnetic $CuFe_2O_4$@Ag@ZIF-8 Nanocomposites with Highly Catalytic Activity Based on Cellulose Nanocrystals. *Molecules* **2020**, *25* (1), 124.

(35) Faraj, R. H.; Ahmed, H. U.; Rafiq, S.; Sor, N. H.; Ibrahim, D. F.; Qaidi, S. M. Performance of Self-Compacting mortars modified with Nanoparticles: A systematic review and modeling. *Cleaner Materials* **2022**, *4*, 100086.

(36) Yonatan Mulushoa, S.; Murali, N.; Tulu Wegayehu, M.; Margarette, S.J.; Samatha, K. Influence of Cu-Cr substitution on

https://doi.org/10.1021/acsomega.3c05764
ACS Omega 2023, 8, 47623−47634

structural, morphological, electrical and magnetic properties of magnesium ferrite. *Results in Physics* **2018**, *8*, 772−779.
(37) Chen, Y.; Zhang, L.; Zhang, H.; Zhong, K.; Zhao, G.; Chen, G.; Lin, Y.; Chen, S.; Huang, Z. Band gap manipulation and physical properties of preferred orientation CuO thin films with nano wheatear array. *Ceram. Int.* **2018**, *44* (1), 1134−1141.
(38) Munir, M. A.; Naz, M. Y.; Shukrullah, S.; Farooq, M. U.; Kamran, K.; Irfan, M.; Ghanim, A. A. J. Testing of magnetic and dielectric traits of microwave plasma treated NiCuZn spinel ferrites for efficient energy storage and high-frequency applications. *Materials Science and Engineering: B* **2023**, *291*, 116374.
(39) Shuib, R. K.; Shamsuddin, R. The use of Bis-(3-triethoxysilylpropyl) tetrasulphane for surface modification of silica, ferrite and kenaf fiber filled natural rubber composites; comparison of aqueous solvent deposition, dry blend and integral blend methods. *J. Appl. Polym. Sci.* **2021**, *138* (36), 50905.
(40) Kumar Sahu, A.; Aravind, R.; Sankhar Brahma, G. Synthesis and investigation of structural, morphological, thermal behaviour, and magnetic properties of $CoFe_2O_4$-MnO_2 nano-composites. *Materials Today: Proceedings* **2022**, *49*, 1762−1768. Bastami, T. R.; Entezari, M. H. Synthesis of manganese oxide nanocrystal by ultrasonic bath: Effect of external magnetic field. *Ultrasonics Sonochemistry* **2012**, *19* (4), 830−840.
(41) Mary Jacintha, A.; Manikandan, A.; Chinnaraj, K.; Arul Antony, S.; Neeraja, P. Comparative studies of spinel MnFe2O4 nanostructures: structural, morphological, optical, magnetic and catalytic properties. *J. Nanosci. Nanotechnol.* **2015**, *15* (12), 9732−9740.
(42) Gandhi, S.; Roy, I. Methylene blue loaded, silica coated cobalt ferrite nanoparticles with potential for combination therapy. *Materials Research Express* **2019**, *6* (7), 074005.
(43) Bajpai, O. P.; Setua, D. K.; Chattopadhyay, S. A brief overview on ferrite (Fe_3O_4) based polymeric nanocomposites: recent developments and challenges. *Journal of Research Updates in Polymer Science* **2015**, *3* (4), 184.
(44) Vareda, J. P. On validity, physical meaning, mechanism insights and regression of adsorption kinetic models. *J. Mol. Liq.* **2023**, *376*, 121416.
(45) Doğaroğlu, Z. G.; Uysal, Y.; Demir, A.; Makas, M. N.; Çaylalı, Z. Synthesis, characterization and optimization of PVA/SA hydrogel functionalized with zeolite (clinoptilolite): Efficient and rapid color removal from complex textile effluents. *Mater. Chem. Phys.* **2023**, *295*, 127090.
(46) Mishra, S.; Sahoo, S. S.; Debnath, A. K.; Muthe, K. P.; Das, N.; Parhi, P. Cobalt ferrite nanoparticles prepared by microwave hydrothermal synthesis and adsorption efficiency for organic dyes: Isotherms, thermodynamics and kinetic studies. *Advanced Powder Technology* **2020**, *31* (11), 4552−4562.
(47) Ren, C.; Ding, X.; Fu, H.; Li, W.; Wu, H.; Yang, H. Core-shell superparamagnetic monodisperse nanospheres based on amino-functionalized $CoFe_2O_4$@SiO_2 for removal of heavy metals from aqueous solutions. *RSC Adv.* **2017**, *7* (12), 6911−6921.
(48) Ghasemi, N.; Ghasemi, M.; Moazeni, S.; Ghasemi, P.; Alharbi, N. S.; Gupta, V. K.; Agarwal, S.; Burakova, I. V.; Tkachev, A. G. Zn (II) removal by amino-functionalized magnetic nanoparticles: Kinetics, isotherm, and thermodynamic aspects of adsorption. *Journal of Industrial and Engineering Chemistry* **2018**, *62*, 302−310.
(49) Azadian, M.; Gilani, H. G. Adsorption of Cu^{2+}, Cd^{2+}, and Zn^{2+} by engineered biochar: Preparation, characterization, and adsorption properties. *Environmental Progress & Sustainable Energy* **2023**, *42* (4), No. e14088.
(50) Christopher, F. C.; Anbalagan, S.; Kumar, P. S.; Pannerselvam, S. R.; Vaidyanathan, V. K. Surface adsorption of poisonous Pb(II) ions from water using chitosan functionalised magnetic nanoparticles. *IET nanobiotechnology* **2017**, *11* (4), 433−442.
(51) Dolgormaa, A.; Lv, C. J.; Li, Y.; Yang, J.; Yang, J. X.; Chen, P.; Wang, H. P.; Huang, J. Adsorption of Cu(II) and Zn(II) Ions from Aqueous Solution by Gel/PVA-Modified Super-Paramagnetic Iron Oxide Nanoparticles. *Molecules* **2018**, *23* (11), 2982.
(52) Azizi, S.; Mahdavi Shahri, M.; Mohamad, R. Green Synthesis of Zinc Oxide Nanoparticles for Enhanced Adsorption of Lead Ions from Aqueous Solutions: Equilibrium, Kinetic and Thermodynamic Studies. *Molecules* **2017**, *22* (6), 831.
(53) Irfan, M.; Zaheer, F.; Hussain, H.; Naz, M. Y.; Shukrullah, S.; Legutko, S.; Mahnashi, M. H.; Alsaiari, M. A.; Ghanim, A. A. J.; Rahman, S. Kinetics and Adsorption Isotherms of Amine-Functionalized Magnesium Ferrite Produced Using Sol-Gel Method for Treatment of Heavy Metals in Wastewater. *Materials* **2022**, *15* (11), 4009.
(54) Fan, H.; Ma, X.; Zhou, S.; Huang, J.; Liu, Y.; Liu, Y. Highly efficient removal of heavy metal ions by carboxymethyl cellulose-immobilized Fe3O4 nanoparticles prepared via high-gravity technology. *Carbohydr. Polym.* **2019**, *213*, 39−49.
(55) Langmuir, I. The adsorption of gases on plane surfaces of glass, mica and platinum. *Journal of the American Chemical society* **1918**, *40* (9), 1361−1403.
(56) Asadi Haris, S.; Dabagh, S.; Mollasalehi, H.; Ertas, Y. N. Alginate coated superparamagnetic iron oxide nanoparticles as nanocomposite adsorbents for arsenic removal from aqueous solutions. *Sep. Purif. Technol.* **2023**, *310*, 123193.
(57) Bao, S.; Tang, L.; Li, K.; Ning, P.; Peng, J.; Guo, H.; Zhu, T.; Liu, Y. Highly selective removal of Zn(II) ion from hot-dip galvanizing pickling waste with amino-functionalized Fe_3O_4@SiO_2 magnetic nano-adsorbent. *J. Colloid Interface Sci.* **2016**, *462*, 235−242.
(58) Li, H.; Xiao, D. l.; He, H.; Lin, R.; Zuo, P. l. Adsorption behavior and adsorption mechanism of Cu(II) ions on amino-functionalized magnetic nanoparticles. *Transactions of Nonferrous Metals Society of China* **2013**, *23* (9), 2657−2665.
(59) Freundlich, H. M. F. Over the adsorption in solution. *J. Phys. Chem.* **1906**, *57*, 152.

https://doi.org/10.1021/acsomega.3c05764
ACS Omega 2023, 8, 47623−47634